J Mater Sci (2022) 57:13403–13413

Composites & nanocomposites

Facile preparation of glycine-based mesoporous graphitic carbons with embedded cobalt nanoparticles

Wenhai Wang[1], Alvaro Y. Tesio[2], Mara Olivares-Marín[3,*], Pedro Gómez Romero[4], and Dino Tonti[1,*]

[1] Institut de Ciència de Materials de Barcelona (ICMAB), Consejo Superior de Investigaciones Científicas (CSIC), Campus UAB, 08193 Bellaterra, Barcelona, Spain
[2] Centro de Investigación y Desarrollo en Materiales Avanzados y Almacenamiento de Energía de Jujuy CIDMEJu (CONICET, Universidad Nacional de Jujuy), Centro de Desarrollo Tecnológico General Savio, 4612 Palpalá, Jujuy, Argentina
[3] Departamento de Ingeniería Mecánica, Energética y de los Materiales, Centro Universitario de Mérida, Universidad de Extremadura, 06800 Mérida, Spain
[4] Catalan Institute of Nanoscience and Nanotechnology (ICN2), The Barcelona Institute of Science and Technology (CSIC-BIST), Campus UAB, 08193 Bellaterra, Barcelona, Spain

Received: 14 March 2022
Accepted: 8 June 2022
Published online: 12 July 2022

ABSTRACT

A simple route has been developed for the preparation of mesoporous graphitic carbons with embedded cobalt nanoparticles just using glycine as a nitrogen source, cobalt nitrate and distilled water. After heating the mixture to 300 °C under magnetic stirring, a dry solid product was obtained, which was then carbonized at 900 °C under argon atmosphere. Changing the glycine/Co molar ratio allowed controlling the size of the cobalt particles and their dispersion in the carbon matrix, the porosity of the carbon and its graphitic character. The carbon–metal composites obtained were tested as oxygen cathodes in Li–O_2 batteries. Cells assembled exhibited a full discharge capacity up to 2.19 mAh cm^{-2} at a current of 0.05 mA cm^{-2} and over 39 cycles at a cutoff capacity of 0.5 mAh cm^{-2}. This work provides a green, feasible and simple way to prepare mesoporous graphitic carbons with embedded cobalt nanoparticles without involving templates.

Handling Editor: Andrea de Camargo.

Address correspondence to E-mail: maraom@unex.es; dino.t@csic.es

https://doi.org/10.1007/s10853-022-07421-3

GRAPHICAL ABSTRACT

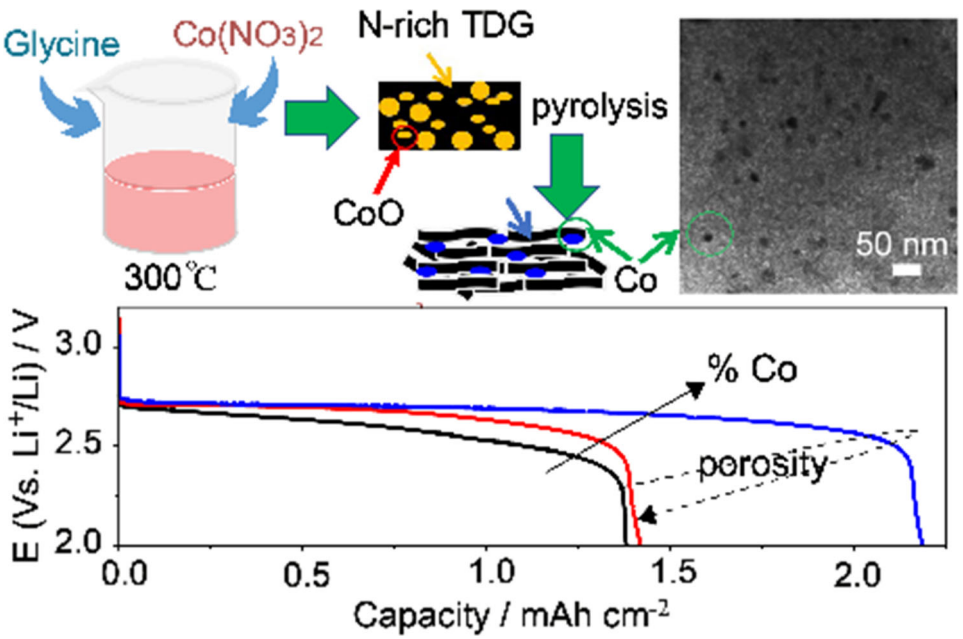

Introduction

In the global challenge of developing more efficient and ecofriendly energy systems, lithium-ion batteries have historically attracted the greatest interest, but today searching for higher energy density, a series of batteries known as "new generation batteries" are emerging. Among them lithium–oxygen battery (Li–O_2) stands out in terms of its energy density [1, 2]. In recent years, the study of various aspects of the non-aqueous Li–O_2 battery has been intensified, covering the stability of the electrolytes, solvents, cathode materials used and the problems derived from the charge/discharge reversibility of the battery (specially the oxidation of ORR products). During the discharge process, O_2 is reduced by a series of mechanisms strongly dependent on current density [3], solvent [4] and nature of the cathode [5] until it forms (mainly) insoluble and insulating Li_2O_2 [6]. However, the loss of capacity and the low cyclability that these batteries present is due to the oxygen species [7, 8] produced in the oxygen reduction and evolution reactions, which are highly reactive and produce parasitic reactions, which decompose the components of the cell [9] such as the cathode [10] and the electrolyte [11].

Without any doubt, one of the most important aspects to developing a Li–O_2 battery is the oxygen cathode. For a Li–O_2 battery, this must fulfill a series of requirements, such as high oxygen permeability, excellent conductivity and catalysis of the oxygen redox reaction. Several non-carbonaceous materials are currently being studied to be used as cathodes [12, 13]. Nonetheless, carbon-based materials remain the most studied materials for cathode application in Li–O_2 batteries, in spite of having many known issues [5].

The known catalytic effect of cobalt has been introduced in Li–O_2 batteries as redox mediators [14, 15], carbon-free cathodes [16, 17] and carbon cathodes [18, 19]. Among the latter, porous carbons with embedded cobalt and cobalt oxide nanoparticles have been widely investigated in the field of energy conversion and storage: lithium-ion batteries [20, 21] lithium–sulfur batteries [22, 23] and Li–O_2 batteries [24, 25]; these last were mainly motivated by their ORR and OER catalytic activity [26]. In fact, it has

been reported that Co nanoparticles embedded in carbon nanostructures can reduce the charge and discharge polarization of Li–O_2 batteries extending its lifetime [27]. Indeed, it can also reduce the charge overvoltage by forming easily decomposable amorphous Li_2O_2 [27].

Several methods have been already proposed for synthesizing Co/porous carbons composites employing numerous carbon precursors, cobalt sources and experimental methods (see Table S1 in Supplementary material). Most of these methods suffer from need of expensive organic precursors (such as cobalt acetylacetonate and potassium hexacyanocobaltate), complicated processing (such as silica, or carbonates as templates) and careful washing. The table below summarizes the strategies used to obtain the Co-carbon composites used for oxygen redox.

Taking into account all the above, in search of a simpler and more sustainable route, we report herein a synthesis process to prepare mesoporous graphitic carbons with embedded cobalt particles to be used as cathodes in Li–O_2 batteries. The synthesis involved the use of commercial glycine, cobalt nitrate and distilled water. Glycine has been used elsewhere as a reducing fuel for the synthesis of ultraporous metals by a simple combustion reaction [28]. We performed an extensive composition and morphology characterization of these materials, named G*X*–Co–T (where *X* represents the glycine amount in the molar ratio G/CoN), and we studied the electrochemical properties. Both the morphological characteristics and the electrochemical behavior of the materials strongly varied depending on the preparation conditions and the amount of Co added. Cells assembled with G6–Co–T delivered a full discharge capacity up to 2.19 mAh cm^{-2} at a current of 0.05 mAh cm^{-2} over 39 cycles without any capacity loss at a cutoff capacity of 0.5 mAh cm^{-2}.

Experimental sections

Synthesis of MGC-Co

Mesoporous graphitic carbons with embedded cobalt nanoparticles (MGC–Co) were prepared by using a two-step simple method with commercial powdered glycine (glycine for synthesis, CAS number 56-40-6, Sigma-Aldrich) and cobalt (II) nitrate hexahydrate (CoN, $Co(NO_3)_2 \cdot 6H_2O$, ACS reagent, ≥ 98%, CAS 10026–22-9, Sigma-Aldrich). The schematic illustration of the synthesis is shown in Scheme 1. Briefly, glycine powder was dissolved in deionized water under stirring using a PYREX® beaker. Subsequently, an amount of CoN was added to the previous solution until it was completely dissolved. Glycine/CoN molar ratios employed are shown in Table S2. Then, the solution was heated up to 300 °C within the same beaker on a digital hot plate stirrer until a brown dark residue was developed, and the release of vapors ended. This step ensured a good dispersion of nitrates in the matrix of the carbon precursor. The nitrogen-rich, thermally decomposed glycine (N-rich TDG) obtained was cooled at room temperature and subsequently carbonized in a tubular furnace at 900 °C under Ar atmosphere for 1 h using a heating rate of 10 °C/min. Before characterization, the carbonized products were grinded in an agate mortar and sieved through a 180-mesh. The average carbon yield was around 15 wt.% MGC-Co and was labeled as G*X*–Co–T, where *X* represents the glycine amount in the molar ratio G/CoN. For comparison purposes, carbonized glycine (G–T) at 900 °C was also prepared as a bare sample. An overview of the samples prepared is provided in Table S2, which also includes the respective Co contents calculated from the ash residues of thermal gravimetry in air (see below for conditions).

Materials characterization

Thermogravimetric analysis (TGA) was carried out with a simultaneous thermogravimetric analysis (TG)-differential scanning calorimetry/differential thermal analysis (heat flow DSC /DTA) system NETZSCH-STA 449 F1 Jupiter. The amount of cobalt incorporated in the carbon materials was analyzed by thermogravimetry from 25 to 900 °C at a heating rate of 5 °C/min under flowing air (80 mL/min). N_2 adsorption/desorption experiments were performed at − 196 °C using a Micromeritics ASAP 2020 equipment. Specific surface areas, S_{BET}, were determined by the Brunauer–Emmett–Teller (BET) method. Micropore volumes (V_{mi}) and external surface areas (S_{ext}) were determined by the *t*-plot method. Total pore volume (V_T) was estimated by the Gurvitsch's rule as the amount adsorbed at a relative pressure of $P/P_0 = 0.995$. Pore size distributions (PSDs) were estimated from the adsorption branches

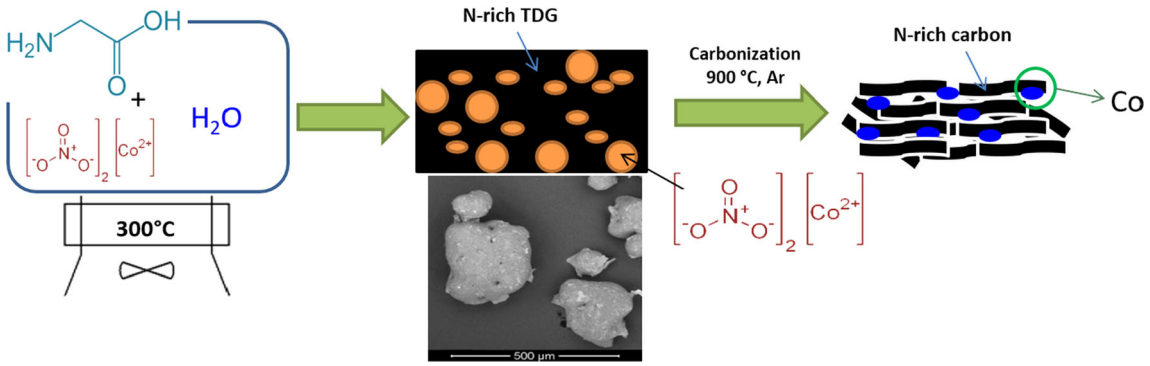

Scheme 1 Synthesis route scheme of mesoporous graphitic carbons with embedded cobalt nanoparticles (MGC-Co).

of the isotherms by the Barrett–Joyner–Halenda (BJH) model. TEM studies were performed with a JEOL (JEM1210) instrument, operating at 100 keV. Before examination, the samples were dispersed in anhydrous ethanol and deposited on a holey carbon film on a copper grid. X-ray diffraction (XRD) patterns at small and wide angles were obtained on a Siemens D5000 instrument operating at 40 kV and 20 mA, using Cu–Ka radiation (l = 0.15406 nm). X-ray photoelectron spectroscopy (XPS) measurements were carried out using a SPECS EA10P hemispherical analyzer using a 300 W non-monochromatic X-ray source (Al Kα line with a photon energy of 1486.6 eV).

Electrochemical measurements

As carbon powders, the different MGC-Co samples synthesized here were used after grinding in a mortar and sieving through a 180-mesh. The method used for the preparation of carbon – binder composite electrodes was based on the common procedure in which a carbon powder is mixed with polyvinylidene fluoride (PVDF, Sigma-Aldrich) as a binder and carbon black (Super P, TIMCAL) in the mass ratio of 4:4:2 in *N*-methyl-2-pyrrolidone (NMP, Sigma-Aldrich, ≥ 99.0%). The slurry obtained was used to impregnate a 10-mm-diameter carbon paper (Freudenberg H2315/H23) and finally dried at 80 °C for 25 h. The electrode loading was of the order of 1 mg (∼ 1.3 mg cm^{-2}). Li–O_2 battery used consisted of a Teflon homemade cell based on the Giessen battery design [29]. The electrolyte was prepared in a glovebox without exposure to air: 1 M lithium triflate (LiTf, Sigma-Aldrich, 99.995%) dissolved in diethylene glycol dimethyl ether (DEGDME, Sigma-Aldrich, 99.5%). The separator was a 12-mm-diameter glass fiber filter (filterLab MFV1, 260 µm thick) soaked with ∼ 100 µl of electrolyte, the anode a 11-mm-diameter Li metal foil (Rockwood Lithium, 0.4 mm thick). All Li–O_2 cells were assembled in an argon-filled glove box. Once assembled, the cell was purged with dry pure oxygen for 60 s. Electrochemical tests, such as cyclic voltammetry and galvanostatic charge–discharge measurements, were performed using a MTI BST8-WA battery tester Biologic VMP3. All the tests were done at 25 °C.

Results and discussion

The literature data [30] indicate that glycine decomposes at temperatures between 220 and 280 °C into glycylglycine (dipeptide) and 2,5-piperazinedione. Among others, NH_3, H_2O and CO_2 gases evolve during the decomposition [30, 31]. At the same time, cobalt nitrate can be reduced to CoO, N_2O and H_2O at around 242 °C [30, 32]. According to that, after this first heating step, the dark product obtained presumably is composed of a complex mixture of glycylglycine (dipeptide), 2,5-piperazinedione and CoO. On the other hand, during the carbonization up to 900 °C, the obtained solid product can decompose releasing CO_2, HCNO, HCN [30] and NH_3 leading to a N-rich carbonaceous product at the end of the process. At the same time, the carbothermal reduction reaction of CoO to elemental metal occurs at temperatures higher than 800 °C [33] resulting in particles of cobalt embedded in the N-rich carbon matrix. Additionally, these metal particles that emerged could act as catalysts for the conversion of amorphous carbon into more ordered or graphitic carbon [34].

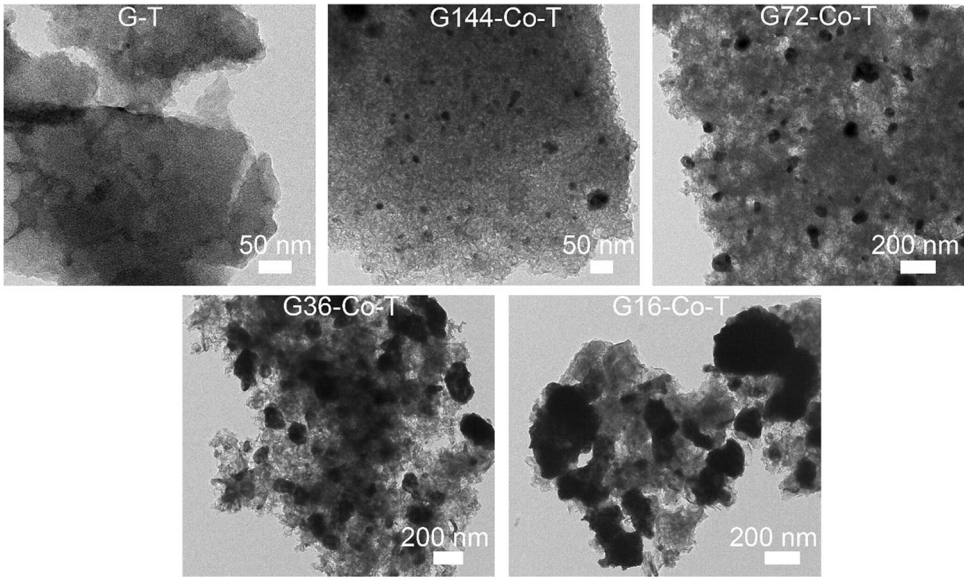

Figure 1 TEM images of G–T and GX–Co–T samples.

The morphology and structure of samples observed by TEM analysis are shown in Fig. 1. TEM image of carbonized glycine (G–T) revealed a carbonaceous material with a dense structure with low porosity. GX–Co-T samples showed clearly embedded cobalt particles within carbon matrix, the sizes and distributions of which are function of G/CoN molar ratio. In addition, all these samples revealed to have certain porosity which are also dependent on cobalt nitrate loading employed during synthesis. For lower G/CoN molar ratios (samples G144–Co–T and G72–Co–T), cobalt particles showed good dispersion and poor agglomeration in the carbon matrix, being the mean Co particle diameter in the range of 50–200 nm. On the other hand, TEM images of samples G36–Co–T, G16–Co–T and G6–Co–T revealed that an increase in the cobalt loading to values higher than 16 wt.% induced the formation of larger cobalt particles (up to about 500 nm) that did not disperse uniformly on the carbon matrix due to a clear agglomeration.

Figure 2a–b shows the N_2 sorption isotherms and the corresponding BJH pore size distributions (PSDs) of GX–Co–T samples. Pristine carbon obtained directly from the carbonization of glycine (G–T) was mainly a microporous carbon that shows a type I isotherm. Nevertheless, the addition of CoN influenced the mesostructuration of final products changing their isotherms shape to type II with associated H3-type hysteresis loop that according to the IUPAC classification indicates the presence of non-rigid aggregates of plate-like particles or assemblies of slit-shaped mesopores [35].

According to textural data calculated from N_2 isotherms (see Table S3), a total pore volume (V_T) maximum is observed with the G36–Co–T (16 wt.% Co), with a V_T 2.3 times compared to pristine carbon G–T. For higher amounts of the experimentally determined Co (and thus of the porogen nitrate precursor), V_T gradually decreased, possibly associated with the high density of Co content and structural degradation (see Fig. 2c). Samples G6–Co–T and G36–Co–T showed clear mesoporous structures compared to pristine carbon. Ordered mesoporous carbons with embedded cobalt nanoparticles made by a novel one-pot laser-assisted approach were reported recently by Chimbeau et al. [35].

The structures of the pristine carbon (G–T) and Co-doped carbons were analyzed by XRD. XRD patterns of samples are shown in Fig. 2d. Sample G–T only presents a weak and broad reflection at around 24° corresponding to the (0 0 2) plane of carbon [36, 37], which indicates a still highly amorphous nature after the thermal treatment. On the other hand, samples prepared using cobalt nitrate showed a diffraction peak at 2θ = 44.2° and 51.5° corresponding to (1 1 1) and (2 0 0) crystal planes of metallic cubic cobalt, respectively. On the other hand, traces of CoO can be also observed due to the oxidation of cobalt particles upon to exposure of air at room temperature [38]. In Fig. 2d, it can be appreciated how the (0 0 2) carbon peak becomes increasingly sharper even when the proportion of cobalt in the sample is small. These

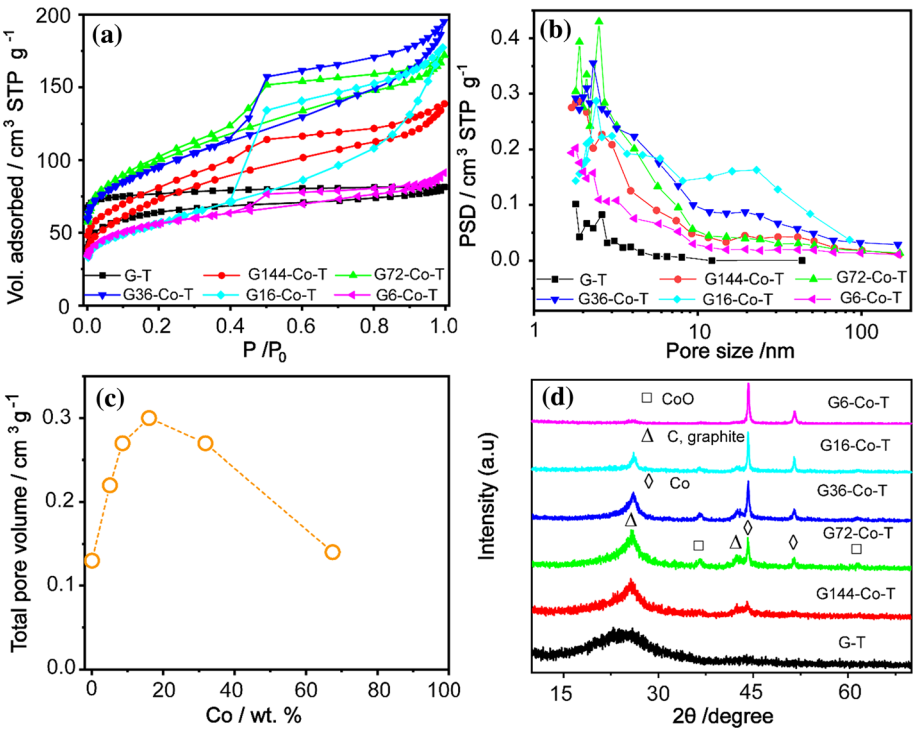

Figure 2 **a** Nitrogen adsorption/desorption isotherms of G–T and GX–Co–T samples; **b** pore size distribution curves from the adsorption branches of the isotherms by BJH. **c** Total pore volume vs. experimentally determined Co content in G–T and GX–Co–T samples; **d** XRD patterns of samples G–T and Co-based samples.

facts corroborate that, as previously reported [34], the formation of metal particles (e.g., Fe, Co and Ni) during carbonization can act as graphitization catalysts at relatively low temperatures. Note that in an uncatalyzed reaction the graphitization process occurs at temperatures above 2000 °C [39].

The XPS spectra in Figure S1 and Fig. 3 show the surface composition of representative samples, which can be qualitatively related to their bulk composition. GT pristine carbon presents a set of peaks corresponding to C 1s (285 eV), N 1s (401 eV) and O 1s (532 eV). Thus, the product obtained directly from the carbonization of glycine (at 900 °C) appears particularly N enriched. C 1 s spectrum can be mainly divided into C–C/C= C (284 eV), C–N (285 eV), C–O (286 eV) and O–C =O (289 eV) [40], which confirms that the carbon is bonded to nitrogen and some oxygen groups. Similarly, the high-resolution N 1 s spectrum can be deconvoluted into pyridinic-N (398 eV), Co–N_x (399 eV), pyrrolic N (400 eV), graphitic N (401 eV) and oxidized N (402 eV) [41, 42]. It is known that pyridinic N and Co–N_x species play an important role for ORR and OER [43]. The total of pyridinic N and Co–N_x of G6–Co–T (37%) is higher than that of G–T (21%) or G36–Co–T (26%) (Table S4). Meanwhile, XPS spectra of samples obtained using cobalt nitrate exhibit in addition new peaks, corresponding to Co(0), Co(II), Co–N_x and the shake-up satellite peaks [44]. In addition, the O 1s spectra also prove the existence of cobalt oxide. The dominant existence of surface Co^{2+} oxides in the XPS analysis can be attributed to the thin CoO layer shell formed by the exposure of cobalt particles to ambient air [38] given the XPS surface sensitivity.

Cyclic voltammetry (CV) was applied to investigate the electrocatalytic activities of selected Co-based carbons and G–T within the voltage range of 2.0–4.5 V (Fig. 4a). All cathodes exhibit a reduction and an oxidation peak, respectively, ascribed to the formation of Li_2O_2 and the decomposition of Li_2O_2, respectively [45]. It is worth noticing that G6–Co–T shows larger ORR and OER peak current than G–T and G36–Co–T, implying its superior ORR and OER activity. Figure 6b shows discharge curves of Li–O_2 batteries at 0.05 mA cm^{-2}. The discharge capacity of G6–Co–T electrode (2.19 mAh cm^{-2}) is much higher than that of G–T electrode (1.38 mAh cm^{-2}) and G36–Co–T electrode (1.42 mAh cm^{-2}) consistent with what is expected from the results of the CV. The excellent performance of G6–Co–T electrode can be attributed to its higher pyridinic N and Co–N_x content, providing more active sites for ORR [43], facilitating the formation and better distribution of the discharge products [46].

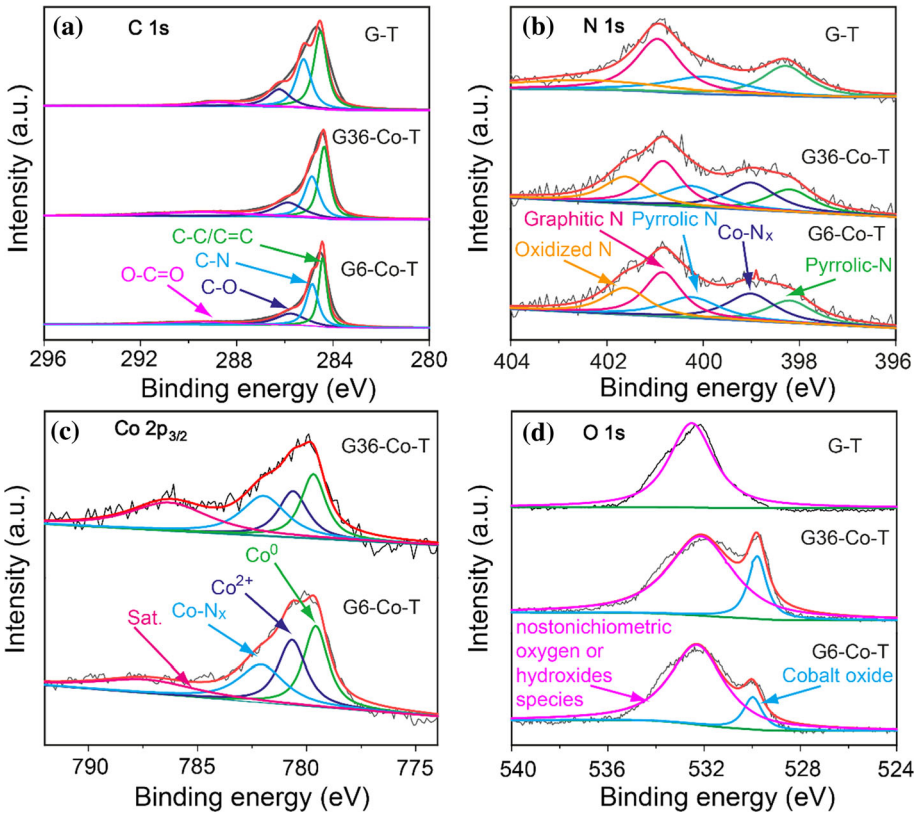

Figure 3 Deconvoluted XPS spectra C 1s (**a**), N 1s (**b**) Co $2p_{3/2}$ (**c**) O 1s (**d**) of G–T, G36–Co–T and G6–Co–T.

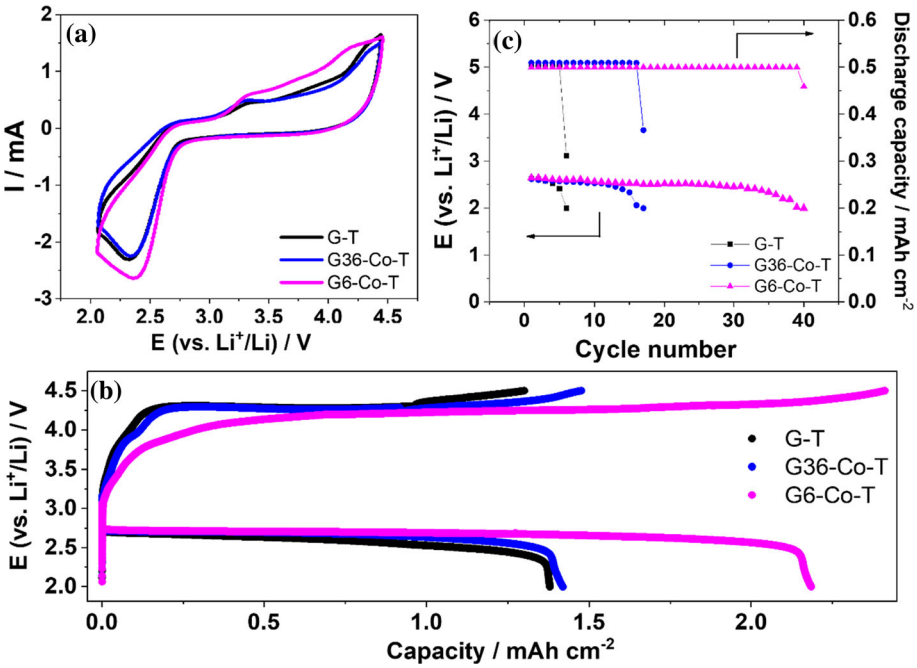

Figure 4 Electrochemical performance of Li $–O_2$ batteries in a 1 M LiTf dissolved in DEGDME electrolyte: **a** CV curves at a scan rate of 20 mV s^{-1}; **b** full discharge–charge profiles at 0.05 mA cm^{-2}; **c** cycling performance with both potential (2.0–4.5 V vs Li^+/Li) and capacity (0.5 mAh cm^{-2}) limitations, showing the terminal voltage and capacity for each cycle.

The cycling performance of the cathode with G-6, G6–Co–T and G36–Co–T was evaluated with the limited capacity of 0.5 mAh cm^{-2} at the current density 0.05 mA cm^{-2} (Fig. 4c). G6–Co–T cathode presents an improved cycle stability, proving once again the benefit of this over the other tested materials. There is an evident improvement on the discharge potential between GT and G36–Co–T. Here, the 2.3 times larger total pore volume may allow maintaining electrochemically active surface area, even though clogging occurs finally after discharging a similar capacity. However, when the percentage of Co increases to 67%, the increase in discharge capacity obtained is very evident (more than 50%). Note that in this case, the pore volume is approximately the same (0.13 ~ 0.14 cm^3 g^{-1}), which justifies that the catalytic effect of the cobalt, together with pyridine nitrogen content added to the increase in the carbon graphitic character, has a more positive effect on the battery discharge than the total pore volume. This catalytic effect could imply a modified discharge mechanism that promotes a more homogeneous distribution of precipitate, which at the same time improves its removal, as confirmed by the enhanced anodic current above 3.2 V vs. Li (Fig. 4a), and by the improved cycle life. The discharge capacity and cycle life of G6–Co–T are comparable to several recently reported cathodes for Li–O_2 batteries (Table S5).

Conclusions

A novel and straightforward synthetic procedure is presented here allowing to produce N-enriched mesoporous graphitic carbon materials embedded with cobalt nanoparticles. This material makes use of the porous structure of a carbon with a high degree of graphitization and also takes the advantage of both catalytic effects of the N and the Co. Li–O_2 cells assembled with G6–Co–T electrode (Co = 67%) exhibited a full discharge capacity up to 2.19 mAh cm^{-2} at a current of 0.05 mAh cm^{-2} and cycle stability for over 39 cycles without capacity loss at a cutoff capacity of 0.5 mAh cm^{-2}.

The reported route is very simple and avoids the problem of residual templates after the reaction, consequently, eliminates the use of strong acids (i.e., HF) to remove the template. For the fact of not using even a wash of the final product, the waste generation is almost absent. In addition, glycine is an abundant and inexpensive raw material in the chemical industry. Carbon obtained directly from the carbonization of glycine was mainly a microporous carbon with low degree of graphitization but significant N content. However, the addition of cobalt nitrate influenced significantly the structure of final products turning it mesoporous. It is important to mention that even with a low proportion of cobalt a high degree of graphitization at low temperature could be reached. Both the porosity and the Co content could be adjusted with the initial ratio of the reagent concentration. For these reasons, this synthetic route can be considered not only economic but also green and eco-friendly.

Acknowledgements

This research was supported by the Spanish Ministry of Science and Innovation, through the "Severo Ochoa" Programme for Centers of Excellence in R&D (CEX2019-000917-S), the projects MAT2017-91404-EXP, RTI2018-096273-B-I00, RTI2018-3097753-B-I00, with FEDER co-funding, the CSIC program for the Spanish Recovery, Transformation and Resilience Plan "Plataforma Temática Interdisciplinar Transición Energética Sostenible+ (PTI-TRANSENER +)" funded by the Recovery and Resilience Facility of the European Union, established by the Regulation (EU) 2020/2094. The authors also acknowledge the Generalitat de Catalunya (2017SGR1687). W.W. gratefully acknowledges the support from the China Scholarship Council (CSC No.:201808340076). This work has been performed within the framework of the doctoral program in materials science of UAB (W. W.).

Funding

Open Access funding provided thanks to the CRUE-CSIC agreement with Springer Nature.

Declarations

Conflict of interest The authors declared that they have no conflict of interest.

Supplementary Information: The online version contains supplementary material available at https://doi.org/10.1007/s10853-022-07421-3.

References

[1] Wang H, Wang X, Li M, Zheng L, Guan D, Huang X, Xu J, Yu J (2020) Porous materials applied in nonaqueous Li-O_2 batteries: status and perspectives. Adv Mater 32:2002559. https://doi.org/10.1002/adma.202002559

[2] Wang Y, Lu Y-C (2020) Nonaqueous lithium-oxygen batteries: Reaction mechanism and critical open questions. Energy Storage Mater 28:235. https://doi.org/10.1016/j.ensm.2020.03.007

[3] Adams BD, Radtke C, Black R, Trudeau ML, Zaghib K, Nazar LF (2013) Current density dependence of peroxide formation in the Li–O_2 battery and its effect on charge. Energy Environ Sci 6:1772. https://doi.org/10.1039/c3ee40697k

[4] Lai J, Liu H, Xing Y, Zhao L, Shang Y, Huang Y, Chen N, Li L, Wu F, Chen R (2021) Local strong solvation electrolyte trade-off between capacity and cycle life of Li-O_2 batteries. Adv Funct Mater 31:2101831. https://doi.org/10.1002/adfm.202101831

[5] Balaish M, Jung JW, Kim ID, Ein-Eli Y (2019) A critical review on functionalization of air-cathodes for nonaqueous Li-O_2 batteries. Adv Funct Mater 30:1808303. https://doi.org/10.1002/adfm.201808303

[6] Cao D, Yu F, Chen Y, Gao X (2021) Improving the true cycling of redox mediators-assisted Li-O_2 Batteries. Energy Environ Mater 4:201. https://doi.org/10.1002/eem2.12185

[7] Mourad E, Petit YK, Spezia R, Samojlov A, Summa FF, Prehal C, Leypold C, Mahne N, Slugovc C, Fontaine O, Brutti S, Freunberger SA (2019) Singlet oxygen from cation driven superoxide disproportionation and consequences for aprotic metal–O_2 batteries. Energy Environ Sci 12:2559. https://doi.org/10.1039/c9ee01453e

[8] Lee HW, Kim H, Jung HG, Sun YK, Kwak WJ (2021) Ambilaterality of redox mediators towards $^1O_2$ in Li-O_2 batteries: trap and quencher. Adv Funct Mater 31:2002559. https://doi.org/10.1002/adfm.202102442

[9] Mozhzhukhina N, Marchini F, Torres WR, Tesio AY, Mendez De Leo LP, Williams FJ, Calvo EJ (2017) Insights into dimethyl sulfoxide decomposition in Li-O_2 battery: understanding carbon dioxide evolution. Electrochem Commun 80:16. https://doi.org/10.1016/j.elecom.2017.05.004

[10] Dong Q, Yao X, Zhao Y, Qi M, Zhang X, Sun H, He Y, Wang D (2018) Cathodically stable Li-O_2 battery operations using water-in-salt electrolyte. Chem 4:1345. https://doi.org/10.1016/j.chempr.2018.02.015

[11] Mehta MR, Knudsen KB, Bennett WR, McCloskey BD, Lawson JW (2021) Li-O_2 batteries for high specific power applications: a multiphysics simulation study for a single discharge. J Power Sources 484:229261. https://doi.org/10.1016/j.jpowsour.2020.229261

[12] X Lu, N Sakai, D Tang, X Li, T Taniguchi, R Ma, T Sasaki (2020) CoNiFe layered double hydroxide/$RuO_{2.1}$ nanosheet superlattice as carbon-free electrocatalysts for water splitting and Li-O_2 batteries. ACS Appl Mater Interfaces 12: 33083. https://doi.org/10.1021/acsami.0c07656

[13] Xing Y, Chen N, Luo M, Sun Y, Yang Y, Qian J, Li L, Guo S, Chen R, Wu F (2020) Long-life lithium-O_2 battery achieved by integrating quasi-solid electrolyte and highly active Pt_3Co nanowires catalyst. Energy Storage Mater 24:707. https://doi.org/10.1016/j.ensm.2019.06.008

[14] Blanchard R, Martin V, Mantoux A, Chatenet M (2018) Cobalt porphyrin and Salcomine as novel redox shuttle species to enhance the oxygen evolution reaction in Li O_2 batteries. Electrochim Acta 261:384. https://doi.org/10.1016/j.electacta.2017.12.129

[15] Li J, Ding S, Zhang S, Yan W, Ma Z-F, Yuan X, Mai L, Zhang J (2021) Catalytic redox mediators for non-aqueous Li-O_2 battery. Energy Storage Mater 43:97. https://doi.org/10.1016/j.ensm.2021.08.036

[16] Qiu X-y, Liu S-j, D-z Xu (2018) Yolk-shell structured Cu_2O as a high-performance cathode catalyst for the rechargeable Li-O_2 batteries. J Mater Sci 53:1318. https://doi.org/10.1007/s10853-017-1555-y

[17] Qian Z, Li X, Wang L, Wu T, Sun B, Du L, Ma Y, Du C, Zuo P, Yin G (2020) Enabling Highly stable Li–O_2 batteries with full discharge–charge capability: the porous binder- and carbon-free IrNi nanosheet cathode. ACS Sustainable Chem Eng 8:16115. https://doi.org/10.1021/acssuschemeng.0c02154

[18] Wang W, Khabazian S, Roig-Sanchez S, Laromaine A, Roig A, Tonti D (2021) Carbons derived from alcohol-treated bacterial cellulose with optimal porosity for Li–O_2 batteries. Renew Energ 177:209. https://doi.org/10.1016/j.renene.2021.05.059

[19] Zhao T, Yao Y, Yuan Y, Wang M, Wu F, Amine K, Lu J (2021) A universal method to fabricating porous carbon for Li-O_2 battery. Nano Energy 82:105782. https://doi.org/10.1016/j.nanoen.2021.105782

[20] Hong SH, Song MY (2018) Syntheses of nano-sized Co-based powders by carbothermal reduction for anode materials of lithium ion batteries. Ceram Int 44:4225. https://doi.org/10.1016/j.ceramint.2017.12.002

[21] Li Q, Wang Y, Yu J, Yuan M, Tan Q, Zhong Z, Su F (2022) High-performance Si-Containing anode materials in lithium-ion batteries: a superstructure of Si@Co–NC composite works effectively. Green Energy Environ 7:116. https://doi.org/10.1016/j.gee.2020.08.007

[22] Wang M, Zhou X, Cai X, Wang H, Fang Y, Zhong X (2020) Hierarchically porous, ultrathin N–doped carbon nanosheets embedded with highly dispersed cobalt nanoparticles as efficient sulfur host for stable lithium–sulfur batteries. J Energy Chem 50:106. https://doi.org/10.1016/j.jechem.2020.03.014

[23] Li J, Chen C, Qin F, Jiang Y, An H, Fang J, Zhang K, Lai Y (2018) Mesoporous Co–N–C composite as a sulfur host for high-capacity and long-life lithium–sulfur batteries. J Mater Sci 53:13143. https://doi.org/10.1007/s10853-018-2566-z

[24] Song J, Lv X, Jiao Y, Wang P, Xu M, Li T, Chen X, Li J, Zhang Z (2018) Catalyst nanoarchitecturing via functionally implanted cobalt nanoparticles in nitrogen doped carbon host for aprotic lithium-oxygen batteries. J Power Sources 394:122. https://doi.org/10.1016/j.jpowsour.2018.05.058

[25] Zhai Y, Wang J, Gao Q, Fan Y, Hou C, Hou Y, Liu H, Shao Q, Wu S, Zhao L, Ding T, Dang F, Guo Z (2019) Highly efficient cobalt nanoparticles anchored porous N-doped carbon nanosheets electrocatalysts for Li-O_2 batteries. J Catal 377:534. https://doi.org/10.1016/j.jcat.2019.07.055

[26] Zhang C, Shu J, Shi S, Nie J, Ma G (2020) Hemp derived N-doped highly porous carbon containing Co nanoparticles as electrocatalyst for oxygen reduction reaction. J Colloid Interface Sci 559:21. https://doi.org/10.1016/j.jcis.2019.09.064

[27] Kim YJ, Lee H, Lee DJ, Park JK, Kim HT (2015) Reduction of charge and discharge polarization by cobalt nanoparticles-embedded carbon nanofibers for Li-O_2 batteries. Chemsuschem 8:2496. https://doi.org/10.1002/cssc.201500520

[28] Gómez-Romero P, Fraile J, Ballesteros B (2013) Fractal porosity in metals synthesized by a simple combustion reaction. RSC Adv 3:2351. https://doi.org/10.1039/c2ra22441k

[29] Bender CL, Hartmann P, Vračar M, Adelhelm P, Janek J (2014) On the thermodynamics, the role of the carbon cathode, and the cycle life of the sodium superoxide (NaO_2) battery. Adv Energy Mater 4:1301863. https://doi.org/10.1002/aenm.201301863

[30] Manukyan KV, Cross A, Roslyakov S, Rouvimov S, Rogachev AS, Wolf EE, Mukasyan AS (2013) Solution combustion synthesis of nano-crystalline metallic materials: mechanistic studies. J Phys Chem C 117:24417. https://doi.org/10.1021/jp408260m

[31] Schaberg A, Wroblowski R, Goertz R (2018) Comparative study of the thermal decomposition behaviour of different amino acids and peptides. J Phys Confer Ser 1107:032013. https://doi.org/10.1088/1742-6596/1107/3/032013

[32] Yuvaraj S, Fan-Yuan L, Tsong-Huei C, Chuin-Tih Y (2003) Thermal decomposition of metal nitrates in air and hydrogen environments. J Phys Chem B 107:1044. https://doi.org/10.1021/jp026961c

[33] L'vov BV (2000) Mechanism of carbothermal reduction of iron, cobalt, nickel and copper oxides. Thermochim Acta 360:109. https://doi.org/10.1016/S0040-6031(00)00540-2

[34] Thambiliyagodage CJ, Ulrich S, Araujo PT, Bakker MG (2018) Catalytic graphitization in nanocast carbon monoliths by iron, cobalt and nickel nanoparticles. Carbon 134:452. https://doi.org/10.1016/j.carbon.2018.04.002

[35] Kim M-Z, Sharma P, Kim Y, Alam SF, Lee HR, Cho CH (2019) One-step template-free hydrothermal synthesis of partially Sr-incorporated hierarchical K-CHA zeolite microspheres. Micropor Mesopor Mat 286:65. https://doi.org/10.1016/j.micromeso.2019.05.007

[36] Yang X, Ding Y, Shen Z, Sun Q, Zheng F, Fong H, Zhu Z, Liu J, Liang J, Wang X (2019) High-strength electrospun carbon nanofibrous mats prepared via rapid stabilization as frameworks for Li-ion battery electrodes. J Mater Sci 54:11574. https://doi.org/10.1007/s10853-019-03698-z

[37] Li D, Han Z, Leng K, Ma S, Wang Y, Bai J (2021) Biomass wood-derived efficient Fe–N–C catalysts for oxygen reduction reaction. J Mater Sci 56:12764. https://doi.org/10.1007/s10853-021-06122-7

[38] Ding S, Xue M, Wu R, Lai Y, Men Y, Kong X, Han L, Han J, Yang W, Yang Y, Du H, Wang C, Yang J (2018) Electron beam reduction induced self-assembly growth of Co/CoO nanocomposite materials. J Alloy Compd 744:615. https://doi.org/10.1016/j.jallcom.2018.02.033

[39] Kinoshita K (1988) Carbon, Electrochemical and Physical Properties. John Wiley & Sons, Chichester, New York, Brisbane, Toronto. https://doi.org/10.1002/bbpc.198800269

[40] Zhang J, Zhu W, Pei Y, Liu Y, Qin Y, Zhang X, Wang Q, Yin Y, Guiver MD (2019) Hierarchically porous Co-N-C cathode catalyst layers for anion exchange membrane fuel cells. Chemsuschem 12:4165. https://doi.org/10.1002/cssc.201901668

[41] Jiang H, Liu Y, Hao J, Wang Y, Li W, Li J (2017) Self-Assembly synthesis of cobalt- and nitrogen-coembedded trumpet flower-like porous carbons for catalytic oxygen reduction in alkaline and acidic media. ACS Sustain Chem Eng 5:5341. https://doi.org/10.1021/acssuschemeng.7b00655

[42] Niu H-J, Wang A-J, Zhang L, Feng J-J (2020) Bioinspired one-step pyrolysis fabrication of 3D Porous Co, N, P-doped carbon nanosheets with enriched CoNx active sites as high-performance bifunctional oxygen electrocatalyst for rechargeable Zn–air battery. ACS Appl Energy Mater 3:2781. https://doi.org/10.1021/acsaem.9b02450

[43] Zhang M, Dai Q, Zheng H, Chen M, Dai L (2018) Novel MOF-derived Co@N-C bifunctional catalysts for highly efficient Zn-air batteries and water splitting. Adv Mater 30:1705431. https://doi.org/10.1002/adma.201705431

[44] Li Y, Mao Z, Wang Q, Li D, Wang R, He B, Gong Y, Wang H (2020) Hollow nanosheet array of phosphorus-anion-decorated cobalt disulfide as an efficient electrocatalyst for overall water splitting. Chem Eng J 390:124556. https://doi.org/10.1016/j.cej.2020.124556

[45] Wang H, Wang H, Huang J, Zhou X, Wu Q, Luo Z, Wang F (2019) Hierarchical mesoporous/macroporous Co-doped NiO nanosheet arrays as free-standing electrode materials for rechargeable Li-O_2 batteries. ACS Appl Mater Interfaces 11:44556. https://doi.org/10.1021/acsami.9b13329

[46] Li C, Liu D, Xiao Y, Liu Z, Song L, Zhang Z (2019) Mesoporous Co_3O_4-rods-entangled carbonized polyaniline nanotubes as an efficient cathode material toward stable lithium–air batteries. ACS Appl Energy Mater 2:2939. https://doi.org/10.1021/acsaem.9b00291